

# The Lieb-Robinson correlation function for long disordered transverse-field Ising chains

Brendan J. Mahoney

*Department of Electrical Engineering  
University of Notre Dame  
Notre Dame, IN 46556, USA*

Craig S. Lent

*Department of Electrical Engineering  
Department of Physics and Astronomy  
University of Notre Dame  
Notre Dame, IN 46556, USA*

(Dated: December 30, 2025)

The transverse-field Ising model is useful for studying interacting qubit arrays. The Lieb-Robinson correlation function can be used to characterize the propagation of quantum information in Ising chains. Considerable work has been done to establish bounds on this correlation function in various circumstances. To actually calculate the value of the correlation function directly typically requires a state space which grows exponentially with system size, and so is intractable for all but relatively small systems. We employ a recently-developed method that enables direct calculation of the value of the Lieb-Robinson correlation function and which scales linearly with system size. This enables the computation for systems with many hundreds of qubits, revealing the propagation of quantum information down the chain. We extend this technique to the problem of Ising chains with randomly disordered coupling strengths. Increasing disorder causes localization of the quantum correlations and halts propagation of quantum information.

**Keywords:** Lieb-Robinson, quantum correlations, entanglement, Ising model, Anderson localization, many-body localization

## I. INTRODUCTION

The spread of information and correlations in quantum many-body systems is constrained in a fundamental way, even in the absence of relativistic causality. Lieb and Robinson showed that for a broad class of lattice Hamiltonians with local interactions, the growth of operator support is effectively limited by a finite velocity [1]. Their analysis considers local operators  $\hat{A}_k$  and  $\hat{B}_m$  acting on distinct subsystems  $k$  and  $m$ , with the time evolution of  $\hat{B}_m$  given in the Heisenberg picture by

$$\hat{B}_m(t) = e^{i\hat{H}t/\hbar} \hat{B}_m(0) e^{-i\hat{H}t/\hbar}. \quad (1)$$

The growth of correlations between the two subsystems can be monitored through the norm of the commutator

$$C_{A,B}(t) = \|[\hat{A}_k, \hat{B}_m(t)]\|. \quad (2)$$

Under general locality conditions, this quantity obeys the Lieb-Robinson bound

$$C_{A,B}(t) \leq K e^{-\mu(d_{k,m} - v_{LR}t)}, \quad (3)$$

where  $d_{k,m}$  is a measure of the distance between the subsystems,  $K$  and  $\mu$  are system-dependent constants and  $v_{LR}$  is the Lieb-Robinson velocity. Out-

side the effective light cone defined by this velocity, the commutator is exponentially small. This result has far-reaching implications, providing rigorous bounds on the locality of non-relativistic quantum dynamics and establishing that correlations and entanglement can only propagate within a finite causal region set by the Lieb-Robinson velocity [2, 3].

Considerable work has since refined and extended this framework. For short-range interacting Hamiltonians, tighter bounds have been obtained using a commutative graph construction [4], with subsequent improvements in related approaches [5, 6]. Other directions have focused on systems with long-range couplings, where power-law interactions give rise to modified, nonlinear light cones [7–11]. These developments highlight the range of settings in which Lieb-Robinson techniques are now applied [12–14].

Disorder represents a distinct and particularly rich direction. Anderson's work established that in one and two dimensions, arbitrarily weak disorder localizes all single-particle states, while in three dimensions a localization transition occurs at finite disorder [15, 16]. This localization arises from quantum interference between closed-loop paths that enhances return probabilities and suppresses transport. In interacting spin systems, the impact of disorder was explored early on in studies of the transverse-field Ising model [17, 18]. Building on

Griffiths' original work on random ferromagnets [19], later analyses revealed how rare, strongly ordered regions can appear inside the disordered phase, producing unusual scaling behavior and strongly affecting the dynamics of the system [20–22].

When disorder is introduced, the standard linear light-cone structure implied by the Lieb–Robinson bound can be substantially modified. General analyses have revealed the emergence of logarithmic light cones in several disordered models, including the XY chain and related spin systems [23–29]. In many of these cases, the commutator obeys a bound of the form

$$C_{A,B}(t) \leq K|t|^\alpha e^{-\frac{d_{k,m}}{\xi}} = K e^{\alpha \log(|t|) - \frac{d_{k,m}}{\xi}}, \quad (4)$$

where  $K$  and  $\xi$  are system-dependent constants that set the overall scale and spatial decay length of correlations, respectively. Here the time dependence enters only as a power-law rather than exponentially, resulting in an effective light cone that expands logarithmically in time. This behavior reflects the suppression of operator and information spreading created by disorder, and provides a characterization of slow entanglement growth and constrained locality in disordered quantum phases. For the XY model with disorder, the Lieb–Robinson correlation function has been shown to be bounded under some conditions by a time-independent envelope [30, 31].

It is usual to study either *bounds* on  $C$ , or to calculate the actual values of  $C$  for relatively small systems. The reason for this is the familiar exponential explosion in the size of the state space for a multi-qubit or spin system.

We focus here on the simplest dynamical system, a one-dimensional transverse-field Ising model (TFIM), with the aim of calculating the value of the Lieb–Robinson (LR) correlation function for large systems and exploring the effects of disorder. To this end, we extend our recently developed method [32] for computing the LR correlation function on regular TFIM chains.

The simplicity of the TFIM model does not mean it is without real-world applications. It is a frequently applicable model for qubit arrays. Systems with thousands of qubits are now becoming available, making it possible to realize and study large many-body systems in controlled settings. Examples include entanglement generation in gate-defined quantum dots [33], coherent evolution in neutral-atom arrays [34], and quantum annealing experiments on large TFIM systems [35]. These developments make efficient theoretical methods for analyzing LR correlations in large systems increasingly important.

The present approach for studying the propagation of quantum correlations should be distinguished

from state-based methods. A common technique is to solve the time-dependent Schrödinger equation for a state that is the ground state of an initial Hamiltonian  $H_0$ . At  $t = 0$ , the Hamiltonian is switched to a new Hamiltonian  $H$ , and the time evolution of the state is calculated, using various exact or approximate means. Such “quench” calculations have the great advantage of yielding all possible information in the quantum state over time. The disadvantages are that the results depend on the initial state and, as usual, are limited by the feasibility of representing the state space adequately. The LR correlation function is state-independent, and so depends only on the system Hamiltonian. It is also a two-time correlation function—the correlation is between one qubit at  $t = 0$  and another at some later time  $t$ .

In Section II, we briefly review Anderson localization in a 1D tight-binding chain, using techniques and visualizations that will apply to the TFIM case. Section III describes the TFIM and the operator Pauli walk method for calculating the LR correlation function. The application of this method to the disordered chain is presented in Section IV.

## II. THE TIGHT-BINDING CHAIN: DISORDER AND ANDERSON LOCALIZATION

We first consider a single particle moving on a 1D chain with no disorder. The Hamiltonian for a tight-binding chain of  $N$  sites can be written

$$\hat{H} = -\gamma \sum_{k=1}^{N-1} \left[ |k+1\rangle\langle k| + |k\rangle\langle k+1| \right] \quad (5)$$

where the hopping matrix element is  $\gamma$ , which we take to be positive. The on-site potentials are taken to be zero because they play no role here; this simply sets the zero of energy. The characteristic time is given by

$$\tau \equiv \frac{\pi\hbar}{\gamma}. \quad (6)$$

In the large  $N$  limit, the energy eigenstates can be labeled by a wavenumber  $q$  and the eigenenergies are given by

$$E(q) = -2\gamma \cos(q). \quad (7)$$

We define the velocity  $v$  as the maximum group velocity, thus

$$v\tau = \tau \frac{1}{\hbar} \left. \frac{\partial E}{\partial q} \right|_{max} = 2\pi. \quad (8)$$

We are interested in the case in which the particle is initially localized on the first site so  $\Psi(k, 0) = \delta_{k,1}$ . We solve for the time-dependent wavefunction by directly performing the unitary transformation

$$\Psi(k, t) = e^{-i\hat{H}t/\hbar} \Psi(k, 0). \quad (9)$$

The probability density at site  $k$  and time  $t$  is then  $P(k, t) = |\Psi(k, t)|^2$ .

Figure 1(a)-(c) shows snapshots of the probability density for a line of  $N = 600$  sites at times  $t/\tau = [5, 10, 15]$ . The probability peak moves down the chain with the velocity given by Eq. (8) (i.e.,  $v = 2\pi$  sites/ $\tau$ ).

To connect with the Ising model that follows, we define

$$P_R(k, t) = \sum_{k'=k+1}^N P(k', t), \quad (10)$$

the probability of finding the particle somewhere to the right of site  $k$  at time  $t$ . Figure 1(d)-(f) shows snapshots of  $P_R$  for the same times as above. The front moves down the chain with velocity  $v$ . The sites ahead of the front do not yet “know” about the particle that was at site 1 at time  $t = 0$ .

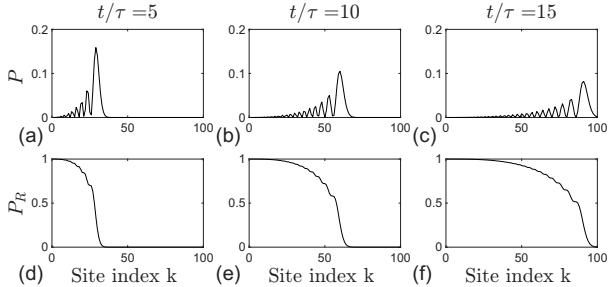


FIG. 1. Snapshots of the probability for a tight-binding chain of 600 sites.  $P(k, t)$ , the probability of finding the particle at site  $k$ , is shown at different times in (a)-(c). The probability  $P_R(k, t)$  of finding the particle to the right of site  $k$  is shown in (d)-(f).

The light-cone plot of  $P_R(k, t)$  for this system is shown in Figure 3(a). The dashed red line corresponds to the front motion. It has a slope of  $1/(2\pi)$  corresponding to the velocity in Eq. (8); because the time is shown on the vertical axis, the front velocity is the inverse of the line’s slope.

We now consider the case where the hopping matrix elements between sites vary randomly down the chain. We are not considering the case with varying on-site potentials simply because variable hopping is most clearly analogous to the TFIM with disordered couplings between spins, which is our primary focus.

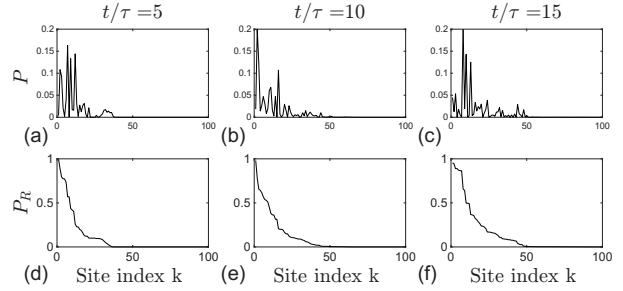


FIG. 2. Snapshots of the probability for the tight-binding chain of 600 sites with disorder. The site probability  $P(k, t)$  is shown in (a)-(c). The probability of finding the particle to the right of site  $k$ ,  $P_R(k, t)$  is shown in (d)-(f). The disorder in the hopping matrix element is characterized by  $\Delta\gamma/\gamma_0 = 1$ .

The Hamiltonian is then

$$\hat{H} = - \sum_{k=1}^{N-1} \gamma_k \left[ |k+1\rangle\langle k| + |k\rangle\langle k+1| \right]. \quad (11)$$

The matrix elements  $\gamma_k$  are independently drawn from a uniform probability distribution centered at  $\gamma_0$  with width  $\Delta\gamma$ :

$$P(\gamma) = \begin{cases} \frac{1}{\Delta\gamma} & \text{for } \gamma \in \left[ \gamma_0 - \frac{\Delta\gamma}{2}, \gamma_0 + \frac{\Delta\gamma}{2} \right], \\ 0 & \text{otherwise.} \end{cases} \quad (12)$$

A particular set of  $N - 1$  randomly chosen  $\gamma_k$ ’s constitutes a specific disorder configuration for the tight-binding chain. We solve for the unitary time evolution of the state function under (11) and compute the probabilities  $P$  and  $P_R$  as before. Figure 2 shows snapshots of the time evolution of both probabilities for a specific disorder configuration chosen from a distribution with  $\Delta\gamma/\gamma_0 = 1$ . The snapshots are at times  $t/\tau = [5, 10, 15]$ , where  $\tau \equiv \pi\hbar/\gamma_0$ . It is clear even in this single sample that, when compared with the non-disordered case of Figure 3(a), the particle propagation is impeded by the multiple reflections caused by the disorder.

Of more interest than the behavior of a specific disorder configuration is the average behavior. We define  $\bar{P}_R$  as the configuration average of  $P_R$ ,

$$\bar{P}_R(k, t) = \frac{1}{N_c} \sum_{m_s}^{N_c} P_R^{(m_s)}(k, t), \quad (13)$$

where  $m_s$  is the index of a specific disorder configuration and  $N_c$  is the total number of such configurations sampled.

Light-cone plots of  $\bar{P}_R$  for the cases of  $\Delta\gamma/\gamma_0 = 1$  (weak disorder) and  $\Delta\gamma/\gamma_0 = 2$  (strong dis-

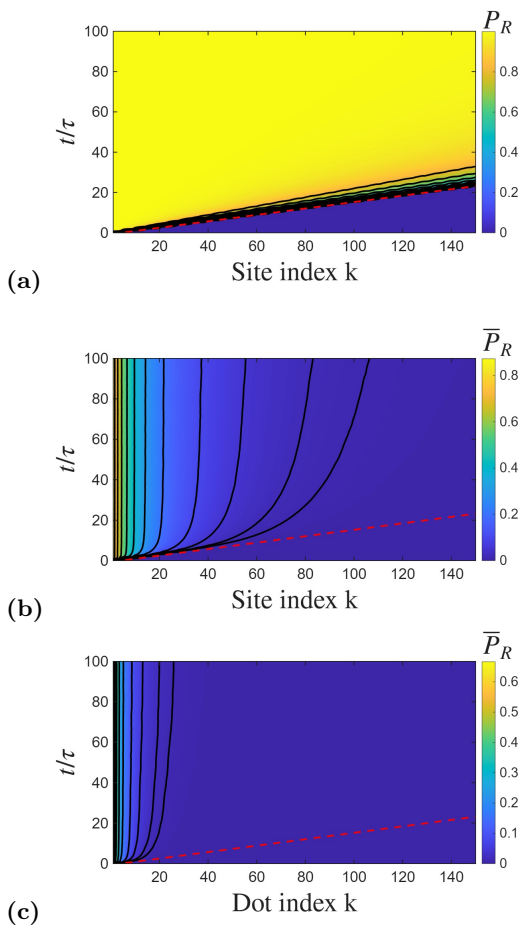


FIG. 3. Light-cone plots for 1D tight-binding chain of 300 sites. (a) The color indicates the site probability  $P(x, t)$  for the case of no disorder,  $\Delta\gamma = 0$ . The color indicates the disorder-averaged probability  $\bar{P}(x, t)$  for (b) weak disorder with  $\Delta\gamma/\gamma = 1$ , and (c) strong disorder with  $\Delta\gamma/\gamma = 2$ . The red dashed line in each plot corresponds to the velocity of Eq. (8).

order) are shown in Figures 3(b) and 3(c) respectively. Here  $N = 300$  sites, though the plots only extend over half that length. The number of disorder configurations in the average is  $N_c=20,000$ . Contours of constant  $\bar{P}_R = [0.01, 0.02, 0.05, 0.1, 0.2, 0.3, 0.4, 0.5, 0.6, 0.7, 0.8]$  are indicated by black lines. The red dashed line in each figure corresponds to ballistic propagation with velocity  $v = 2\pi/\tau$  as seen in Figure 3(a).

The light-cone plots of Figures 3(b) and 3(c) reveal that the disorder suppresses particle motion. This is the well-established single-particle Anderson localization in 1D. The light-cone curves (isocontours of  $\bar{P}_R$ ) are bent upward by the presence of the disorder. Their shape is neither linear nor logarithmic. As time goes on, they in fact become vertical, indicating no further motion down the chain—zero

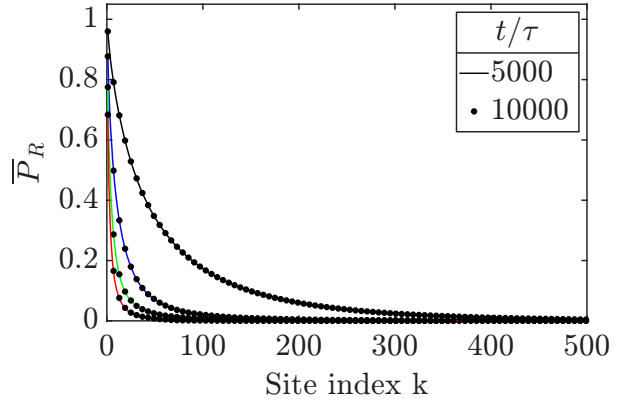


FIG. 4. Configuration averaged probability  $\bar{P}_R$  for two long times. The average is over 2000 sample configurations and  $N = 600$ . The disorder is characterized by  $\Delta\gamma/\gamma_0 = 0.5$  (black), 1 (blue), 1.5 (green) and 2 (red).

propagation velocity.

This can be seen more explicitly by considering  $\bar{P}_R$  at very long times. Figure 4 shows  $\bar{P}_R$  for two long times,  $t/\tau = 5,000$  and  $10,000$ , calculated for four different values of the probability distribution width. For each probability distribution, the result at the two times is identical, indicating that by these times there is no particle transport down the chain.

### III. OPERATOR PAULI WALK METHOD FOR THE ISING CHAIN

#### A. Transverse field Ising model

We consider a 1D chain of  $N_q$  interacting qubits in states  $|0\rangle$  or  $|1\rangle$ , or equivalently of spins  $|\downarrow\rangle$  and  $|\uparrow\rangle$  (we will use the description interchangeably). The system is described by the transverse-field Ising model (TFIM) Hamiltonian with nearest-neighbor couplings:

$$H = -J \sum_{k=1}^{N_q-1} Z_k Z_{k+1} - \gamma \sum_{k=1}^{N_q} X_k, \quad (14)$$

Here  $J$  denotes the coupling energy between qubits; we take  $J \geq 0$ . For a spin system, the  $X$  term can represent an applied transverse magnetic field. We interpret it here equivalently as representing the kinetic energy associated with the flipping dynamics of each qubit or spin. The presence of this term means that an isolated  $|1\rangle$  (or  $|\uparrow\rangle$ ) state is not a stationary state, but will precess in time. A natural timescale, related to the Rabi oscillation time for an isolated qubit, is in terms of the quantity

$$\tau = \frac{\pi\hbar}{\gamma}. \quad (15)$$

It is helpful then to measure time in terms of  $\tau$  and energy in terms of  $\gamma$ . We define the dimensionless Hamiltonian

$$H' \equiv H/\gamma = -J' \sum_{k=1}^{N_q-1} Z_k Z_{k+1} - \sum_{k=1}^{N_q} X_k. \quad (16)$$

where  $J' \equiv J/\gamma$ .

The TFIM has two quantum phases separated by a critical point at  $J' = 1$ . Figure 5(a) shows the ground state and first excited state energies for the system in the  $N_q \rightarrow \infty$  thermodynamic limit.

For  $J' \leq 1$  we say the system is in the *paramagnetic* phase. When  $J' = 0$ , the chain consists of noninteracting spins whose energy eigenstates are each eigenstates of  $X_k$ : the symmetric ground state  $|X^+\rangle = (|\uparrow\rangle + |\downarrow\rangle)/\sqrt{2}$  or antisymmetric excited state  $|X^-\rangle = (|\uparrow\rangle - |\downarrow\rangle)/\sqrt{2}$ . The ground state of the chain consists of all spins in the ground state. The first excited state of the system consists of a single site excited to the  $|X^-\rangle$  state, which costs an energy  $2\gamma$ . As the coupling  $J'$  is turned on, a single excitation on one site can move down the chain, delocalizing and lowering the energy. In this regime, we can think of the system quasiparticles as being roughly these mobile excitations.

For  $J' > 1$ , the system is in the *ferromagnetic* phase. For  $J \gg \gamma$ , the ground state of the whole chain consists of all sites in  $|\uparrow\rangle$  state or all in the  $|\downarrow\rangle$  state. The  $Z_2$  symmetry (flipping all the spins) produces a two-fold degenerate ground state. For finite  $J' > 1$ , we can think of the quasiparticle excitations as domain walls in the chain:  $|\cdots \uparrow\uparrow\downarrow\downarrow \cdots\rangle$ . The motion of the domain wall is enabled by the nonzero kinetic energy term.

For both the paramagnetic and ferromagnetic phases with  $0 < J' < \infty$ , actual system eigenstates are delocalized combinations of these excitations, which mix the character of the simple quasiparticle descriptions above.

For an infinite chain, or one with periodic boundary conditions, the TFIM can be mapped onto an equivalent fermion problem using the Jordan-Wigner transformation [36–38]. A subsequent Bogoliubov transformation rotates the fermion creation and annihilation operators to yield a free fermion Hamiltonian with quasiparticle excitation spectrum

$$E(q) = 2J\sqrt{g^2 + 1 - 2g\cos q}. \quad (17)$$

Here  $q$  is the wavenumber of the harmonic excitation and  $g \equiv 1/J'$ . The energy eigenvalues for the system are all possible combinations of the quasiparticle excitation energies given by Eq. (17). The corresponding quasiparticle group velocities can be calculated via the usual expression  $v(q) = (1/\hbar)\partial E/\partial q$ . The

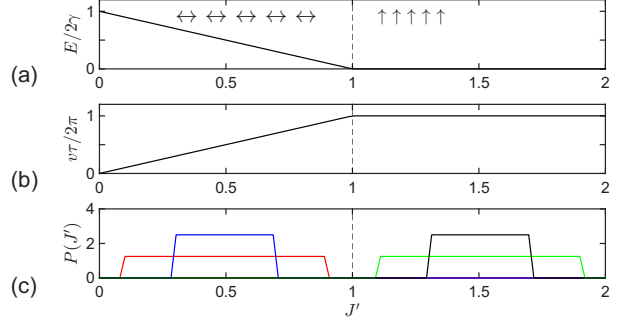


FIG. 5. Two phases of the TFIM chain. (a) Energies of the ground state and first excited state as a function of coupling  $J'$ . For  $J' < 1$ , the system is in the paramagnetic state; for  $J' > 1$  it is in the ferromagnetic state. (b) Front velocity as a function of the coupling  $J'$  given by Eq. (18). (c) Probability distributions for disordered couplings as given by Eq. (30)

maximum value over  $q$  of this velocity is given by

$$v\tau = \begin{cases} 2\pi J' & J' \leq 1 \\ 2\pi & J' > 1. \end{cases} \quad (18)$$

A derivation is given in [32]. Figure 5(b) shows this velocity as a function of  $J'$ . As we will see below, this velocity represents the velocity of the correlation front which propagates down the chain; we therefore refer to it as the front velocity. In the context of quantum chaos, it is also known as the butterfly velocity.

There is another velocity which characterizes the propagation of the first-order effect of correlations, discussed in [32, 39], but it reflects the initial turn-on of extremely small values of correlation and will not concern us here.

## B. Operator Pauli walk method for the Lieb–Robinson correlation function

To characterize the dynamic spread of correlations, we study the Lieb–Robinson correlation function

$$C_k(t) = \|[Z_1(t), Z_k]\|, \quad (19)$$

which quantifies how correlations propagate as a function of time.

The operator  $Z_1(t)$  evolves under  $\hat{H}$  according to

$$Z_1(t) = e^{i\hat{H}t/\hbar} Z_1 e^{-i\hat{H}t/\hbar} \quad (20)$$

or equivalently

$$Z_1(t) = \sum_{n=0}^{\infty} \frac{1}{n!} \pi^n i^n \left(\frac{t}{\tau}\right)^n \left[ \left(\hat{H}'\right)^n, Z_1 \right]. \quad (21)$$

Here we use the standard notation for nested commutators

$$[(A)^n, B] \equiv \underbrace{[A, \dots [A, [A, B] \dots]]}_{n \text{ times}}. \quad (22)$$

which represents  $n$  successive commutations of the operator  $A$  with  $B$ . From the definition in Eq. (19), we see that at  $t = 0$ ,  $Z_1$  commutes with itself, and also with  $Z_k$ , which acts on a different site  $k$ , so  $C_k(0) = 0$ . The time evolution of Eq. (21) results in  $Z_1(t)$  spreading to include components of Pauli operators on other sites. It follows from the Pauli operator commutation relations (e.g.  $[Z, X] = 2iY$ ) that the maximum value of  $C_k(t)$  is 2.

For relatively short chains it is tractable to calculate  $C_k(t)$  directly from Eq. (19) and Eq. (20). This requires calculating the matrix exponential of the  $2^{N_q} \times 2^{N_q}$  Hamiltonian matrix. The result for a ten-qubit line is shown in Figure 6. The correlation initially turns on for each site as the quantum influence propagates down the chain. The effect of reflections from the end of the chain, however, quickly becomes apparent, and indeed dominant. The computational challenge here is the same as that for direct state-based calculations, namely that the size of the operators scales as  $2^{N_q}$ , so for even modestly large systems direct calculations like this become untenable. For example, Colmenarez and Luitz [10] use heroic methods to calculate systems with  $N_q = 22$ .

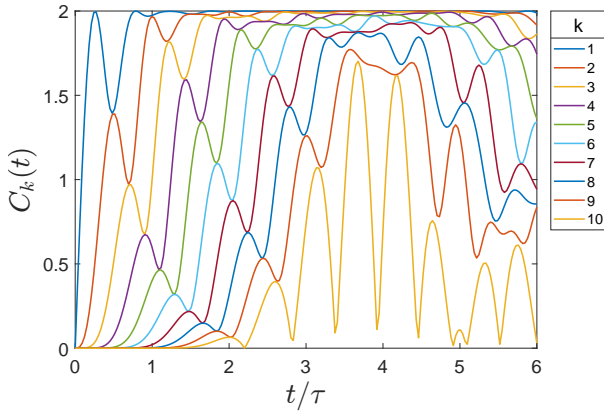


FIG. 6. The Lieb–Robinson correlation function for the TFIM of a ten-qubit chain with  $J' = 1/2$ . This is the result of a direct calculation using the definition of Eq. (19) and the Heisenberg equation of motion of Eq. (20).

Equations (19) and Eq. (21) provide the conceptual foundation for the operator Pauli walk (OPW) method introduced in [32] which addresses the problem of handling longer system sizes. A Pauli string is the tensor product of operators  $I_k, X_k, Y_k$ , or  $Z_k$  on each site; it is usual to suppress the identity operators notationally. Each nested commutation of  $\hat{H}'$

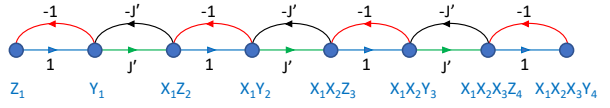


FIG. 7. Pauli operator walk for a four-qubit TFIM chain. The nodes correspond to the eight operator strings listed in (24), and the directed edges represent the value of commutators between  $Z_1$  and terms in  $H'_{4q}$  that appear in Eq. (21)

with  $Z_1$  generates a new Pauli string, corresponding to a “step” in an abstract operator space whose nodes represent Pauli strings and whose edges encode their coupling under  $\hat{H}'$ . The space of Pauli strings has dimension  $4^{N_q}$  and in general the whole space is required to support  $Z_1(t)$  and therefore calculate  $C_k(t)$ . The OPW method exploits the fact that for the TFIM Hamiltonian  $H'$ , the nested commutations in Eq. (21) explore only a much smaller structured subspace of size  $2N_q$  forming a discrete walk that fully captures the dynamics.

To briefly illustrate, consider a four-qubit homogeneous chain governed by

$$H'_{4q} = -J' \sum_{k=1}^3 Z_k Z_{k+1} - \sum_{k=1}^4 X_k. \quad (23)$$

Starting from  $Z_1$ , evaluating any number of successive nested commutators with  $H'_{4q}$  in Eq. (21) generates only eight distinct Pauli strings:

$$Z_1, Y_1, X_1 Z_2, X_1 Y_2, X_1 X_2 Z_3, X_1 X_2 Y_3, X_1 X_2 X_3 Z_4, X_1 X_2 X_3 Y_4. \quad (24)$$

These eight operators form the nodes of closed Pauli operator walks, shown schematically in Fig. 7. The weight of each directed edge represents the value of a commutator in the expansion given by Eq. (21). The sum in (21) maps onto a sum over all walks on the operator chain. Successive commutations alternate between two types of transitions: local rotations induced by the  $X_k$  terms, which generate a weight of 1, and coupling-driven transitions generated by the  $Z_k Z_{k+1}$  interaction terms, which generate a weight  $J'$ . Note that the walk is not along the qubit chain, but rather in this operator space. Thus, the nested commutators needed to calculate  $Z_1(t)$  using Eq. (21) under the Ising Hamiltonian explore only a compact, linearly-connected subset of the full, exponentially larger, space of Pauli strings.

The operator walks can be described using an ad-

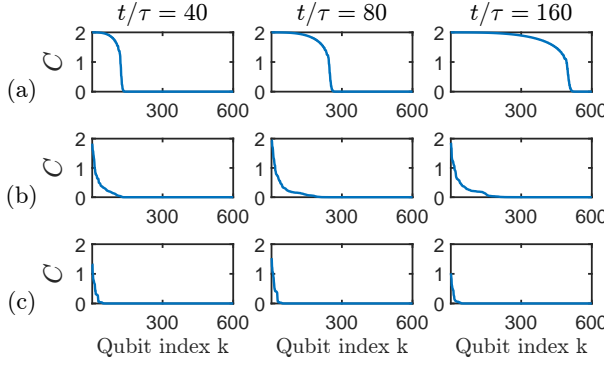


FIG. 8. Snapshots of the time evolution of  $C_k(t)$  for a TFIM chain in the paramagnetic (weak-coupling) phase with  $J'_0 = 0.5$ . (a) No disorder,  $\Delta J' = 0$ . (b) Weak disorder,  $\Delta J' = 0.4$ . (c) Strong disorder,  $\Delta J' = 0.8$ . The chain is 1200 qubits long, but only the first 600 qubits are plotted.

adjacency matrix which takes the tridiagonal form

$$\mathbf{A}_0 = \begin{pmatrix} 0 & 1 & 0 & 0 & 0 & 0 & \cdots & 0 \\ -1 & 0 & J' & 0 & 0 & 0 & \cdots & 0 \\ 0 & -J' & 0 & 1 & 0 & 0 & \cdots & 0 \\ 0 & 0 & -1 & 0 & J' & 0 & \cdots & 0 \\ 0 & 0 & 0 & -J' & 0 & \ddots & \vdots & \vdots \\ 0 & 0 & 0 & 0 & \ddots & \ddots & J' & 0 \\ \vdots & \vdots & \vdots & \vdots & \cdots & -J' & 0 & 1 \\ 0 & 0 & 0 & 0 & \cdots & 0 & -1 & 0 \end{pmatrix}. \quad (25)$$

The alternating 1 and  $J'$  entries along the tridiagonal reflect the alternating  $X$ -induced and  $ZZ$ -induced steps in the operator walk. As shown in [32], summing over all walks governed by this adjacency matrix yields the following closed-form expression for the LR correlation function on the homogeneous chain:

$$C_k^0(t) = \sqrt{\sum_{m=2k}^{2N_q} \left| 2 \left[ \exp \left( -2\pi \frac{t}{\tau} \mathbf{A}_0 \right) \right]_{1,m} \right|^2}. \quad (26)$$

Evaluating Eq. (26) requires calculating matrix exponentials of  $\mathbf{A}_0$ , a sparse real skew-symmetric matrix of size  $2N_q \times 2N_q$ . Using this approach, the LR correlation function can be calculated directly for any time without time-marching or Trotterization. Because Eq. (25) scales only with  $2N_q$ , rather than  $4^{N_q}$ , this approach allows  $C_k(t)$  to be calculated for chains of hundreds or even thousands of qubits. As we shall see below, for many problems a finite chain can be long enough that the results essentially produce those of a semi-infinite chain.

Figure 8(a) shows snapshots of the LR correlation function  $C_k^0(t)$  calculated using the OPW method at

three different times. The Ising chain here is composed of  $N_q = 1200$  qubits, though the correlation function is shown only for the first 600. In this case,  $J' = 0.5$  so the system is in the paramagnetic phase. The front of quantum correlation moves smoothly down the line with the velocity given by Eq. (18) (i.e.,  $v = \pi$  qubits/ $\tau$ ).

#### IV. DISORDERED ISING CHAINS

We now generalize the homogeneous Ising chain to include spatially-varying couplings. Working in the same dimensionless units, the inhomogeneous TFIM is

$$H' = - \sum_{i=1}^{N_q-1} J'_k Z_k Z_{k+1} - \sum_{k=1}^{N_q} X_k, \quad (27)$$

where  $J'_k$  is the coupling between sites  $k$  and  $k+1$ , which we again take to be non-negative but which can now vary down the chain. As in the homogeneous case, the nested-commutator dynamics of  $Z_1(t)$  given by Eq. (19) is confined to a  $2N_q$ -dimensional operator subspace rather than the full  $2^{N_q}$ -dimensional space of all Pauli strings. The only change is that the operator-space adjacency matrix acquires position-dependent weights:

$$\mathbf{A} = \begin{pmatrix} 0 & 1 & 0 & 0 & 0 & 0 & \cdots & 0 \\ -1 & 0 & J'_1 & 0 & 0 & 0 & \cdots & 0 \\ 0 & -J'_1 & 0 & 1 & 0 & 0 & \cdots & 0 \\ 0 & 0 & -1 & 0 & J'_2 & 0 & \cdots & 0 \\ 0 & 0 & 0 & -J'_2 & 0 & \ddots & \vdots & \vdots \\ 0 & 0 & 0 & 0 & \ddots & \ddots & J'_{N_q-1} & 0 \\ \vdots & \vdots & \vdots & \vdots & \cdots & -J'_{N_q-1} & 0 & 1 \\ 0 & 0 & 0 & 0 & \cdots & 0 & -1 & 0 \end{pmatrix}. \quad (28)$$

Thus, the solution to the inhomogeneous problem requires only a straightforward substitution  $\mathbf{A}_0 \rightarrow \mathbf{A}$ . We sum over walks on the same set of operators; only the edge weights of the Pauli walk change. The LR correlation function therefore retains the same closed form, just in terms of the matrix  $\mathbf{A}$ :

$$C_k(t) = \sqrt{\sum_{m=2k}^{2N_q} \left| 2 \left[ \exp \left( -2\pi \frac{t}{\tau} \mathbf{A} \right) \right]_{1,m} \right|^2}. \quad (29)$$

Within this inhomogeneous framework, we construct specific instances of disordered chains by independently sampling each coupling  $J'_k$  from a probability distribution. We use a uniform probability density centered at a baseline coupling  $J'_0$  with width

$\Delta J'$ :

$$P(J') = \begin{cases} \frac{1}{\Delta J'} & \text{for } J' \in \left[J'_0 - \frac{\Delta J'}{2}, J'_0 + \frac{\Delta J'}{2}\right], \\ 0 & \text{otherwise.} \end{cases} \quad (30)$$

Figure 5(c) illustrates the disorder distributions used in this paper. For the paramagnetic phase, we consider two cases centered at  $J'_0 = 0.5$ : a weak-disorder distribution with  $\Delta J' = 0.4$  (blue) and a strong-disorder distribution with  $\Delta J' = 0.8$  (red). For the ferromagnetic phase, we use two analogous distributions centered at  $J'_0 = 1.5$ , with  $\Delta J' = 0.4$  (black) and  $\Delta J' = 0.8$  (green).

### A. Paramagnetic phase

We focus first on the results for the LR correlation function  $C_k(t)$  in the paramagnetic (weak-coupling) phase, taking a baseline coupling of  $J'_0 = 0.5$ .

Figure 8(b) shows snapshots of the LR correlation function  $C_k(t)$  on a 1200-qubit chain (only the first 600 qubits are shown) for a specific random distribution of couplings drawn from Eq. (30) with  $J'_0 = 0.5$  and  $\Delta J' = 0.4$ . Figure 8(c) shows the case of  $\Delta J' = 0.8$ . Increasing disorder in the coupling between qubits clearly impedes propagation of quantum correlations down the chain.

We define the disorder-averaged LR correlation function

$$\overline{C}_k(t) = \frac{1}{N_c} \sum_{m=1}^{N_c} C_k^{(m)}(t), \quad (31)$$

where each  $C_k^{(m)}(t)$  is evaluated from Eq. (29) using one of  $N_c$  independently sampled disorder configurations  $\{J'_i\}^{(m)}$ . This allows us to characterize the effect of disorder overall, independent of the specifics of a particular configuration of couplings.

Figure 9(a) shows the light-cone plot for the reference situation with no disorder,  $\Delta J' = 0$ , and  $J'_0 = 0.5$ . The color of the plot represents the value of  $C_k(t)$  for this chain of 1200 qubits (600 are shown). Isocontours of  $C$  are shown for  $C = [1, 0.9, 0.8, 0.7, 0.6, 0.5, 0.4]$ . They are closely spaced together in this plot, but are indicated for comparison with the disordered cases below. The red dashed line corresponds to the propagation velocity given by Eq. (18). (Note that the slope of the line is the inverse of the velocity.) The light-cone plot is a fuller visualization of the snapshots of the moving correlation front in Figure 8(a).

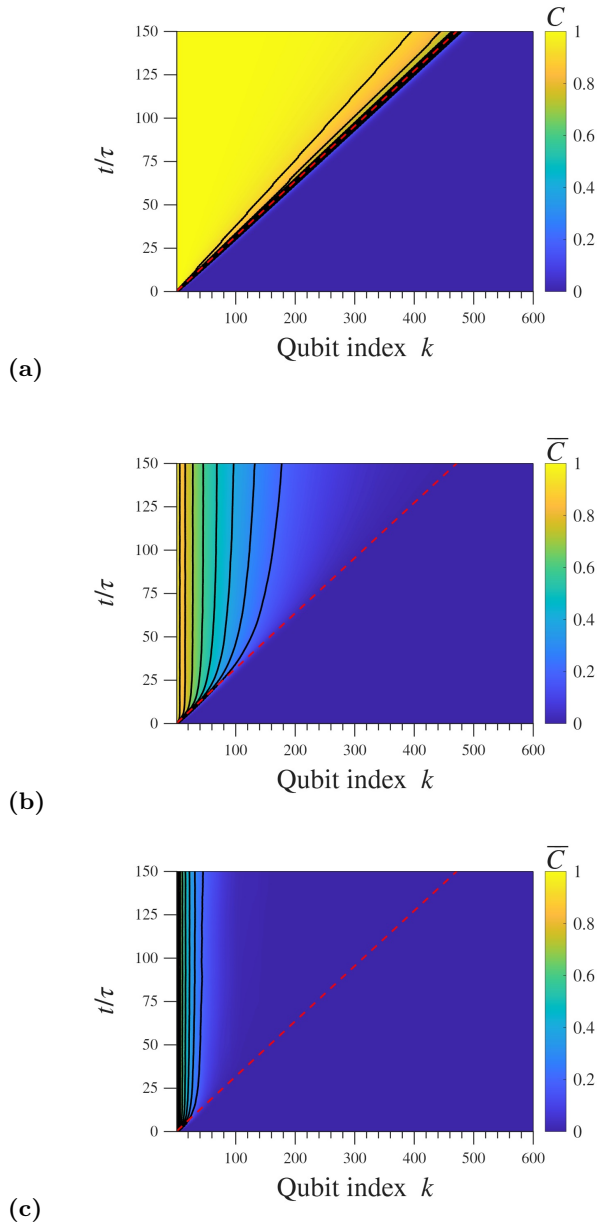


FIG. 9. Light-cone diagrams for Ising chain in the paramagnetic phase,  $J' = 0.5$ , with (a) no disorder,  $\Delta J' = 0$ , (b) weak disorder,  $\Delta J' = 0.4$ , and (c) strong disorder,  $\Delta J' = 0.8$ .

Figure 9(b) shows the light-cone plot for a 600 qubit disordered Ising chain with  $J'_0 = 0.5$  and  $\Delta J' = 0.4$ . Here the color represents the configuration-averaged LR correlation function  $\overline{C}$  defined in Eq. (31), averaged over  $N_c = 500$  configurations. The probability density from which the values of  $J'_k$  are drawn is shown schematically in Figure 5(c) in red. Isocontours are shown for the values of  $\overline{C} = [1, 0.9, 0.8, 0.7, 0.6, 0.5, 0.4]$ . The dashed red

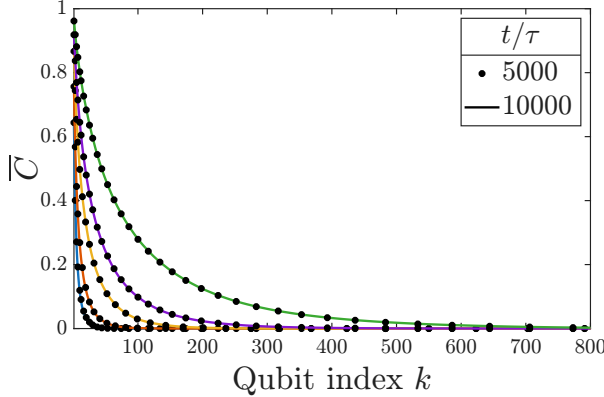


FIG. 10. Disorder-averaged LR correlation function in the paramagnetic phase for two late times. The TFIM chain is 1000 qubits in length with baseline coupling  $J'_0 = 0.5$ .  $\bar{C}(k, t)$  is averaged over 1000 disorder configurations. Results are shown at  $t/\tau = 5,000$  and  $t/\tau = 10,000$ , for different disorder strengths:  $\Delta J' = 0.1$  (green),  $\Delta J' = 0.2$  (purple),  $\Delta J' = 0.4$  (yellow),  $\Delta J' = 0.6$  (red), and  $\Delta J' = 0.8$  (blue). The identity of the two late-time curves (dots and lines) indicates that the penetration of quantum correlations down the chain in each case has become stationary.

line in the light-cone plot again represents the velocity of the front in the disorder-free case. Close to the origin, the  $\bar{C}$  isocontours follow the disorder-free velocity line, but they soon bend upward and the front velocity slows. As time progresses, the isocontours become closer and closer to vertical. This signifies that the front has stopped advancing: correlations become stationary in space, marking the onset of localization.

The high-disorder light-cone, with  $\Delta J' = 0.8$ , is shown in Figure 9(c). The probability density from which the values of  $J'_k$  are drawn is shown as the green curve in Figure 5(c). The  $\bar{C}$  isocontours in this case almost immediately turn vertical, corresponding to no propagation of the correlation front.

The light-cone plots in Figure 9 extend to time  $t/\tau = 150$ . If many-body localization has stopped the propagation of quantum correlations down the chain, we would expect to see the correlation function at longer times become stationary, *i.e.*, independent of time. We can check this by examining  $\bar{C}$  at two much longer times. Figure 10 shows the disorder-averaged LR correlation function for times  $t/\tau = 5,000$  (dots) and  $t/\tau = 10,000$  (solid lines). Here we use a chain of  $N_q = 1000$  qubits and average over  $N_c = 1000$  disorder configurations. The results are shown for various amounts of disorder:  $\Delta J' = [0.1, 0.2, 0.4, 0.6, 0.8]$ . The fact that the dots fall on the lines indicates that in each case the dynamics of the system has localized quantum corre-

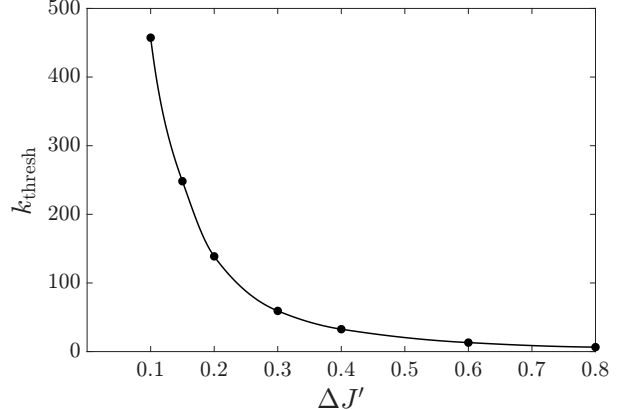


FIG. 11. Localization length as a function of the coupling disorder. The system is 1000 qubits long with  $J'_0 = 0.5$  and the disorder is averaged over  $N_c = 1000$  configurations. The analysis is for a late time, here  $t/\tau = 10,000$ , by which point the LR correlation function has become stationary, as shown in Figure 10. For each disorder strength  $\Delta J'$ ,  $k_{\text{thresh}}$  is the index of the first qubit for which  $\bar{C}_k$  drops below a threshold value, here 0.2. The decreasing trend of  $k_{\text{thresh}}$  with  $\Delta J'$  quantifies the increasing spatial confinement of correlations as disorder grows. The smooth curve is a guide to the eye.

lations that are no longer moving down the chain—zero propagation velocity.

In both the light-cone plots of Figure 9 and the later-time curves of Figure 10, it is clear that higher amounts of disorder (larger  $\Delta J'$ ) result in shorter localization lengths. For example, in the  $\Delta J' = 0.1$  case shown in Figure 10,  $\bar{C}$  is substantial out to several hundred qubits, whereas when  $\Delta J' = 0.8$ , it is extinguished a few tens of qubits down the chain. This observation can be made quantitative by calculating the qubit index for which  $\bar{C}$  first drops below a threshold level for a late time, here chosen to be  $t_{\text{late}}/\tau = 10,000$ . We define  $C_{\text{thresh}}$  as the threshold level (we use 0.2 below) and the corresponding qubit index  $k_{\text{thresh}}$ ,

$$k_{\text{thresh}}(\Delta J') \equiv \min \left\{ k \geq 1 : \bar{C}_k(t_{\text{late}}) \leq C_{\text{thresh}} \right\}. \quad (32)$$

The quantity  $k_{\text{thresh}}$  then quantifies an effective localization length. Figure 11 shows  $k_{\text{thresh}}$  as a function of the disorder strength  $\Delta J'$ . The values are derived from the same 1000-qubit chain described in Figure 10. The results exhibit a clear monotonic decrease of  $k_{\text{thresh}}$  with increasing  $\Delta J'$ , demonstrating that stronger disorder confines quantum correlations to shorter distances.

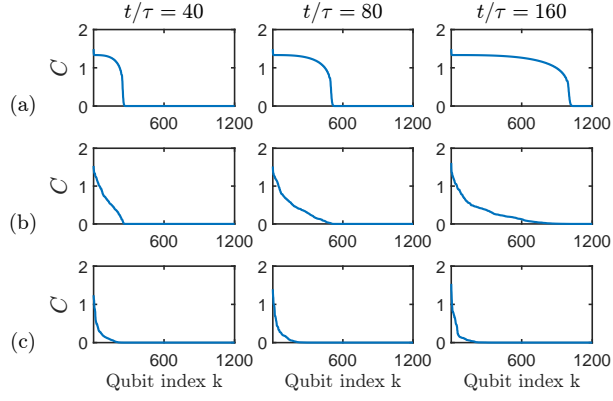


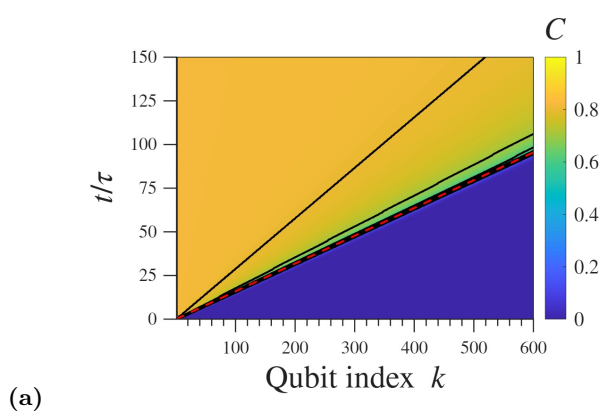
FIG. 12. Snapshots of the time evolution of  $C_k(t)$  for a TFIM chain in the ferromagnetic (strong-coupling) phase with  $J'_0 = 1.5$ . (a) No disorder,  $\Delta J' = 0$ . (b) Weak disorder,  $\Delta J' = 0.4$ . (c) Strong disorder,  $\Delta J' = 0.8$ .

### B. Ferromagnetic phase

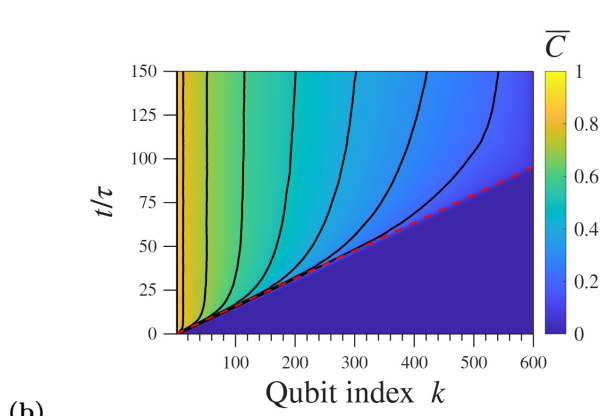
Figure 12(a) shows snapshots of the LR correlation function at three times for a 1200-qubit TFIM chain in the ferromagnetic phase,  $J'_0 = 1.5$ , with no disorder,  $\Delta J' = 0$ . The quantum correlation front moves smoothly down the line with the velocity given by Eq. (18) (i.e.,  $v = 2\pi$  qubits/ $\tau$ ), faster than in the paramagnetic case shown in Figure 8(a).

Figure 12(b) and (c) show snapshots of  $C_k(t)$  for the same length chain and  $J'_0 = 1.5$ , but with coupling disorder characterized by  $\Delta J' = 0.4$  and  $\Delta J' = 0.8$ , respectively. These are each shown for one specific disorder configuration, drawn independently from the probability distribution of Eq. (30). We see that in the ferromagnetic phase, not only is the propagation faster than in the paramagnetic phase, but the quantum correlation penetrates down the chain farther. Higher disorder still impedes propagation and localizes the correlated region nearer the origin.

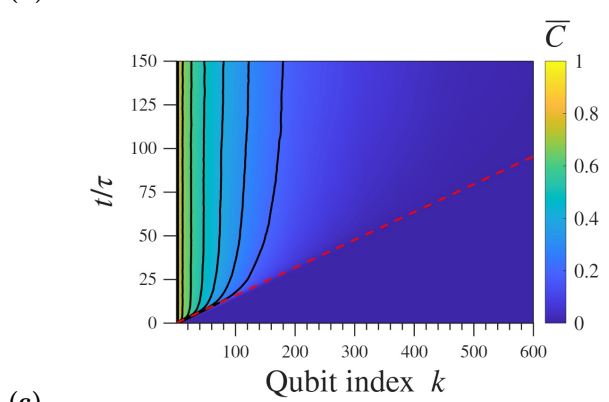
Figure 13(a) shows the light-cone plot of  $C_k(t)$  for a disorder-free 600-qubit chain in the ferromagnetic phase with  $J'_0 = 1.5$ . The color map represents the magnitude of the LR correlation function, and the overlaid isocontours are for levels  $C = [1, 0.9, 0.8, 0.7, 0.6, 0.5, 0.4]$ , though they are hard to separate visually. The red dashed line corresponds to the correlation front velocity of Eq. (18).



(a)



(b)



(c)

FIG. 13. Light-cone plots for Ising chain in the ferromagnetic phase,  $J' = 1.5$  with (a) no disorder,  $\Delta J' = 0$ , (b) weak disorder,  $\Delta J' = 0.4$ , and (c) strong disorder,  $\Delta J' = 0.8$ .

Figure 13(b) and (c) are light-cone plots of the disorder-averaged LR correlation function  $\bar{C}_k(t)$  with  $N_c = 500$ . As above,  $J'_0 = 1.5$  and  $\Delta J' = 0.4$  for the lower-disorder case, with  $\Delta J' = 0.8$  for the higher-disorder case. Isocontours of  $\bar{C}$  for the same levels as above are indicated. The red dashed line shows the front velocity for the disorder-free case. These light-cones are qualitatively similar to those for the paramagnetic case shown in Figure 9. In

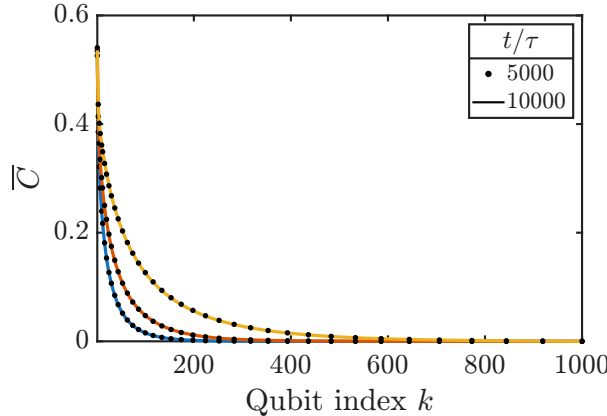


FIG. 14. Disorder-averaged LR correlation function in the ferromagnetic phase for late two late times. The TFIM chain is 1000 qubits in length with baseline coupling  $J'_0 = 1.5$ .  $\bar{C}(k, t)$  is averaged over 1000 disorder configuration. Results are shown at  $t/\tau = 5,000$  and  $t/\tau = 10,000$  for different disorder strengths:  $\Delta J' = 0.4$  (yellow),  $\Delta J' = 0.6$  (red), and  $\Delta J' = 0.8$  (blue). The identity of the two late-time curves (dots and lines) indicates that the penetration of quantum correlations down the chain in each case has become stationary. Compared to the weak-coupling (paramagnetic) case shown in Figure 10, correlations penetrate farther down the chain, corresponding to a larger localization length in the ferromagnetic phase.

the absence of disorder, the correlation front moves ballistically down the chain, yielding straight lightcones. Disorder in the couplings causes the lightcones to bend upward and become vertical. The principal differences between the propagation in the two phases are due to the higher speed of propagation of correlations in the ferromagnetic case, and the greater distances down the chain that the correlations are able to penetrate before being suppressed by the disorder.

As in the paramagnetic case, we can compare the LR correlation function at two late times to confirm that the propagation of quantum correlations has indeed ceased. Figure 14 shows the disorder-averaged correlation function  $\bar{C}(k, t)$  at  $t/\tau = 5,000$  (dots) and  $t/\tau = 10,000$  (solid line) for a 1000-qubit system, averaged over  $N_c = 1000$  disordered configurations, with  $\Delta J' = [0.4, 0.6, 0.8]$ . The results indicate that the spatial profile has reached its stationary form. Again, it is clear that relative to the paramagnetic results of Figure 10, the ferromagnetic correlations decay more slowly in  $k$  at each  $\Delta J'$ , indicating that correlations extend farther from the origin and the effective localization length is larger in the strong-coupling phase.

Hamza, Sims, and Stolz (HSS) found that under certain conditions, the LR correlation function for

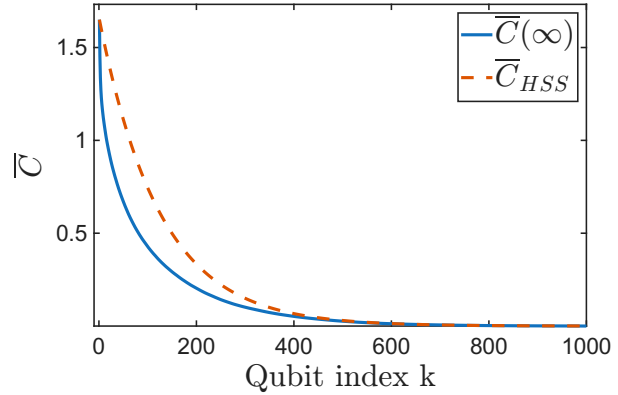


FIG. 15. Comparison between the disorder-averaged late-time LR correlation function and the exponential bound of Hamza, Sims, and Stolz (HSS) [Eq. (33)].

the disordered XY model (of which the Ising model is a special case) has a stationary exponential bound

$$C_k(t) \leq K e^{-\alpha(k-1)}, \quad (33)$$

where  $\alpha$  is a characteristic decay constant [30, 31]. To compare this bound to our result, we evaluate the stationary disorder-averaged correlation profile  $\bar{C}_k(t_{\text{late}})$  at time  $t_{\text{late}}/\tau = 10,000$ . Figures 10 and 14 established that by this time the correlation front has ceased to propagate, so we can use  $\bar{C}_k$  at  $t_{\text{late}}$  to represent the stationary correlation profile  $\bar{C}(\infty)$ . We then determine the largest decay constant  $\alpha$  for which the inequality in Eq. (33) holds for all qubit indices  $k$  with  $\bar{C}_1(t_{\text{late}}) = K$ . Figure 15 compares this exponential bound with our results for a 1000-qubit chain in the ferromagnetic phase with  $J'_0 = 1.5$ ,  $\Delta J' = 0.8$ , and  $N_c = 1000$ . These results conform to the HSS bound, but it is noticeable that the calculated correlations decay significantly faster. This holds for both strong and weak correlations in both paramagnetic and ferromagnetic phases.

## V. DISCUSSION

Seeing the precise form that the Lieb–Robinson correlation function takes as quantum correlations move down a long Ising chain can be very revealing. This calculation is crucially enabled by the operator Pauli walk method [32]. Figures 14 and 15 show calculations on a 1000-qubit chain. To represent either a quantum state or quantum operators on the chain would require a basis of size  $2^{1000} \approx 10^{301}$ , a number that greatly exceeds the number of particles in the visible universe. By contrast, evaluating Eq. (29) for  $C_k(t)$  requires a basis size of only 2000. This is all the more important for assessing directly the effects of disorder because of the need to average over

many random configurations. Of course, the quantum state contains vastly more information than the correlation function.

As we have seen, another feature of the OPW result in Eq. (29) beyond treating arrays that are very long, is that it can be used to compute the LR correlation function at any time, including very long times, without time-marching or Trotterization. This makes it possible to see directly that the light-cones for the disordered Ising chain are not logarithmic, but in fact become vertical (zero-velocity), in agreement with the bound of Hamza, Sims, and Stolz [30, 31].

The analysis of the single-particle tight-binding chain in Section II illustrated the key features of disorder-induced localization using the same approach we subsequently employed in Section IV. The parallels are instructive, but it would be a mis-

take to over-interpret this and conclude that the many-body localization seen in the TFIM is just the Anderson localization of a quasiparticle. The full excitation spectrum of the TFIM Hamiltonian includes the presence of all possible quasiparticles. We have not limited the analysis to the transport of a single quasiparticle; all are included in the correlation function. Similarly, there is no restriction to only low-energy excitations. The localization in this many-body system must be localization of all quasiparticle excitations.

The primary result of this work is the calculation of the Lieb-Robinson correlation function, rather than a bound on it, in the case of disorder. Quantum correlations and information are localized and not able to propagate farther down the chain. Extending the techniques that made this possible is a subject for further study.

---

[1] E. Lieb and D. Robinson, The finite group velocity of quantum spin systems, *Commun. Math. Phys.* **28** (1972).

[2] M. B. Hastings and T. Koma, Spectral gap and exponential decay of correlations, *Communications in Mathematical Physics* **265**, 781–804 (2006).

[3] B. Nachtergaelie, Y. Ogata, and R. Sims, Propagation of correlations in quantum lattice systems, *J. Stat. Phys.* **124** (2006).

[4] Z. Wang and K. R. Hazzard, Tightening the Lieb-Robinson bound in locally interacting systems, *PRX Quantum* **1**, 010303 (2020).

[5] A. Braida, S. Martiel, and I. Todinca, Tight Lieb-Robinson Bound for approximation ratio in quantum annealing, *npj Quantum Inf.* **10**, 40 (2024).

[6] B. Hinrichs, M. Lemm, and O. Siebert, On Lieb-Robinson bounds for a class of continuum fermions, *Ann. Henri Poincaré* **26**, 41 (2025).

[7] R. Sweke, J. Eisert, and M. Kastner, Lieb-Robinson bounds for open quantum systems with long-ranged interactions, *J. Phys. A: Math. Theor.* **52**, 424003 (2019).

[8] L. Colmenarez and D. J. Luitz, Lieb-Robinson bounds and out-of-time order correlators in a long-range spin chain, *Phys. Rev. Res.* **2**, 043047 (2020).

[9] L. Cevolani, G. Carleo, and L. Sanchez-Palencia, Spreading of correlations in exactly solvable quantum models with long-range interactions in arbitrary dimensions, *New J. Phys.* **18**, 093002 (2016).

[10] M. C. Tran, C.-F. Chen, A. Ehrenberg, A. Y. Guo, A. Deshpande, Y. Hong, Z.-X. Gong, A. V. Gorshkov, and A. Lucas, Hierarchy of linear light cones with long-range interactions, *Phys. Rev. X* **10**, 031009 (2020).

[11] J. T. Schneider, J. Despres, S. J. Thomson, L. Tagliacozzo, and L. Sanchez-Palencia, Spreading of correlations and entanglement in the long-range transverse ising chain, *Phys. Rev. Res.* **3**, L012022 (2021).

[12] J.-B. Bru and W. de Siqueira Pedra, *Lieb-Robinson bounds for multi-commutators and applications to response theory*, Vol. 13 (Springer, 2016).

[13] C.-F. A. Chen, A. Lucas, and C. Yin, Speed limits and locality in many-body quantum dynamics, *Rep. Prog. Phys.* **86**, 116001 (2023).

[14] C.-F. Chen and A. Lucas, Optimal frobenius light cone in spin chains with power-law interactions, *Phys. Rev. A* **104**, 062420 (2021).

[15] P. W. Anderson, Absence of diffusion in certain random lattices, *Phys. Rev.* **109**, 1492 (1958).

[16] J. Fröhlich and T. Spencer, Absence of diffusion in the Anderson tight binding model for large disorder or low energy, *Commun. Math. Phys.* **88**, 151 (1983).

[17] B. M. McCoy and T. T. Wu, Theory of a two-dimensional Ising model with random impurities. I. Thermodynamics, *Phys. Rev.* **176**, 631 (1968).

[18] P. Pfeuty, An exact result for the 1D random Ising model in a transverse field, *Phys. Lett. A* **72**, 245 (1979).

[19] R. B. Griffiths, Nonanalytic behavior above the critical point in a random Ising ferromagnet, *Phys. Rev. Lett.* **23**, 17 (1969).

[20] F. Iglói and C. Monthus, Strong disorder RG approach of random systems, *Phys. Rep.* **412**, 277 (2005).

[21] J. Kisker and A. P. Young, Dynamical critical properties of the random transverse-field Ising spin chain, *Phys. Rev. B* **58**, 14397 (1998).

[22] J. A. Hoyos and T. Vojta, Dissipation effects in random transverse-field Ising chains, *Phys. Rev. B* **85**, 174403 (2012).

[23] C. K. Burrell and T. J. Osborne, Bounds on the speed of information propagation in disordered quantum spin chains, *Phys. Rev. Lett.* **99**, 167201 (2007).

[24] M. Friesdorf, *Closed Quantum Systems and Localization*, Ph.D. thesis, University of Cologne, Cologne, Germany (2015), phD Thesis.

[25] Y. Zeng, A. Hamma, Y.-R. Zhang, Q. Liu, R. Li, H. Fan, and W.-M. Liu, Logarithmic light cone, slow entanglement growth, and quantum memory, *Phys. Rev. B* **112**, 094202 (2025).

[26] C. L. Baldwin, A. Ehrenberg, A. Y. Guo, and A. V. Gorshkov, Disordered Lieb-Robinson bounds in one dimension, *PRX Quantum* **4**, 020349 (2023).

[27] C. L. Baldwin, Subballistic operator growth in spin chains with heavy-tailed random fields, *Phys. Rev. B* **111**, 184204 (2025).

[28] M. Gebert and M. Lemm, On polynomial Lieb-Robinson bounds for the XY chain in a decaying random field, *J. Stat. Phys.* **164**, 667 (2016).

[29] D. Damanik, M. Lemm, M. Lukic, and W. Yessen, On anomalous Lieb-Robinson bounds for the Fibonacci XY chain, *J. Spectr. Theory* **6**, 601 (2016).

[30] E. Hamza, R. Sims, and G. Stoltz, Dynamical localization in disordered quantum spin systems, *Commun. Math. Phys.* **315**, 215 (2012).

[31] H. Abdul-Rahman, B. Nachtergael, R. Sims, and G. Stoltz, Localization properties of the disordered XY spin chain, *Ann. Phys.* **529**, 1600280 (2017).

[32] B. J. Mahoney and C. S. Lent, Lieb-Robinson correlation function for the quantum transverse-field Ising model, *Phys. Rev. Res.* **6**, 023286 (2024).

[33] P. Steinacker, T. Tanttu, W. H. Lim, *et al.*, Bell inequality violation in gate-defined quantum dots, *Nat. Commun.* **16**, 3606 (2025).

[34] N. C. Chiu, E. C. Trapp, J. Guo, *et al.*, Continuous operation of a coherent 3,000-qubit system, *Nature* (2025).

[35] A. D. King, A. Nocera, M. M. Rams, J. Dziarmaga, R. Wiersema, W. Bernoudy, J. Raymond, N. Kaushal, N. Heinsdorf, R. Harris, K. Boothby, F. Altomare, M. Asad, A. J. Berkley, M. Boschnak, K. Chern, H. Christiani, S. Cibere, J. Connor, M. H. Dehn, R. Deshpande, S. Ejtemaei, P. Farre, K. Hamer, E. Hoskinson, S. Huang, M. W. Johnson, S. Kortas, E. Ladizinsky, T. Lanting, T. Lai, R. Li, A. J. R. MacDonald, G. Marsden, C. C. McGeoch, R. Molavi, T. Oh, R. Neufeld, M. Norouzpour, J. Pasvolsky, P. Poitras, G. Poulin-Lamarre, T. Prescott, M. Reis, C. Rich, M. Samani, B. Sheldan, A. Smirnov, E. Sterpka, B. Trullas Clavera, N. Tsai, M. Volkmann, A. M. Whiticar, J. D. Whittaker, W. Wilkinson, J. Yao, T. J. Yi, A. W. Sandvik, G. Alvarez, R. G. Melko, J. Carrasquilla, M. Franz, and M. H. Amin, Beyond-classical computation in quantum simulation, *Science* **388**, 199 (2025).

[36] E. Lieb, T. Schultz, and D. Mattis, Two soluble models of an antiferromagnetic chain, *Annals of Physics* **16**, 407 (1961).

[37] S. Sachdev, *Quantum Phase Transitions*, 2nd ed. (Cambridge University Press, 2011).

[38] F. Igloi and G. Tóth, Entanglement witnesses in the XY chain: Thermal equilibrium and postquench nonequilibrium states, *Phys. Rev. Res.* **5**, 013158 (2023).

[39] B. J. Mahoney and C. S. Lent, The value of the early-time Lieb-Robinson correlation function for qubit arrays, *Symmetry* **14** (2022).